Computers, Materials & Continua CMC, vol.62, no.1, pp.17-35, 2020

Multiscale Analysis of the Effect of Debris on Fretting Wear Process Using a Semi-Concurrent Method

Shengjie Wang[1], Tongyan Yue[2] and Magd Abdel Wahab[3, 4, *]

Abstract: Fretting wear is a phenomenon, in which wear happens between two oscillatory moving contact surfaces in microscale amplitude. In this paper, the effect of debris between pad and specimen is analyzed by using a semi-concurrent multiscale method. Firstly, the macroscale fretting wear model is performed. Secondly, the part with the wear profile is imported from the macroscale model to a microscale model after running in stage. Thirdly, an effective pad's radius is extracted by analyzing the contact pressure in order to take into account the effect of the debris. Finally, the effective radius is up-scaled from the microscale model to the macroscale model, which is used after running in stage. In this way, the effect of debris is considered by changing the radius of the pad in the macroscale model. Due to the smaller number of elements in the microscale model compared with the macroscale model containing the debris layer, the semi-concurrent method proposed in this paper is more computationally efficient. Moreover, the results of this semi-concurrent method show a better agreement with experimental data, compared to the results of the model ignoring the effect of debris.

Keywords: Fretting wear, debris, multiscale analysis, semi-concurrent.

1 Introduction

Fretting is a phenomenon in which the micro amplitude oscillatory movement happens between contact surfaces [Klaffke (1989); Yue and Wahab (2017)]. According to the amplitude of relative slip between two contact surfaces, fretting can be classified as: a) stick regime, b) partial slip regime and c) gross sliding regime [Ovcharenko and Etsion (2009)]. Relative slip is complemented by the deformation of the contact surface in stick regime and there is no significant relative slip. In mixed stick and slip regime, there is only a small relative slip at the edge of the contact zone, while in gross sliding regime, there is relative slip across the whole contact zone.

There are many kinds of damages in the fretting process, among which the main ones are fretting wear and fretting fatigue [Berthier, Vincent and Godet (1989)]. Cracks are mostly

[1] Soete Laboratory, Faculty of Engineering and Architecture, Ghent University, Technologiepark Zwijnaarde 903, Zwijnaarde B-9052, Belgium.

[2] State Grid Xinyuan Maintenance Branch, Beijing, China.

[3] Division of Computational Mechanics, Ton Duc Thang University, Ho Chi Minh City, Vietnam.

[4] Faculty of Civil Engineering, Ton Duc Thang University, Ho Chi Minh City, Vietnam.

[*] Corresponding Author: Magd Abdel Wahab. Email: magd.abdelwahab@tdtu.edu.vn.

caused by fretting fatigue in a partial slip regime [Hills (1994)]. A lot of research on the prediction of fatigue [Bhatti, Pereira and Wahab (2018); Bhatti, Pereira and Wahab (2019); Bhatti and Wahab (2018a); (2018b)] and crack propagation [Pereira and Wahab (2018); Pereira and Wahab (2017)] has been reported in literature. Fretting wear plays a key part in gross slip regime. To quantify the wear in fretting process, Archard's equation [Achard (1953); McColl, Ding and Leen (2004); Van Beek (2015)] and the dissipated energy equation [Fouvry, Duo and Perruchaut (2004); Paulin, Fouvry and Deyber (2005)] are mostly used.

Fretting wear is a complex phenomenon because there are many factors that have influences on its process, such as materials, stress field, environment, temperature, loading frequency etc. In fretting process, material removal occurs on contact surfaces, making debris trapped between two contact surfaces. In this way, wear mode is converted from two-body abrasive wear to three-body [Berthier, Vincent and Godet (1989)].

Wear in fretting process is commonly modeled based on finite element method (FEM) due to its efficiency and applicability [McColl, Ding and Leen (2004); Paulin, Fouvry and Meunier (2008)]. To make the simulation more accurate, the effect of the debris is analysed by many researchers. Yue et al. [Yue and Abdel Wahab (2016)] quantified the effect of the debris layer on fretting wear process using a 2D finite element (FE) model. In this model, the debris was set to be a constant, e.g., 5 μm, 10 μm, and 15 μm. In this paper, the effect of the debris was only considered for 500 cycles and the wear kinetics was not considered. Ding et al. [Ding, McColl, Leen et al. (2007)] also proposed a FE based method to analyze the effect of the debris in the fretting wear model. In this model, the introduction and ejection of debris were all considered. The debris thickness was always changing in the fretting process. Yue et al. [Yue and Abdel Wahab (2016)] and Ding et al. [Ding, McColl and Leen (2007)] only analyzed the effect of the debris generated from the specimen, however the debris generated from another contact part was not analyzed. Arnaud et al. [Arnaud, Fouvry and Garcin (2017)] proposed a model to simulate fretting wear that could consider the wear of both contact parts.

The models mentioned above analyzed the effect of debris in a fretting wear process, but it is time-consuming and can cause divergence problems to consider debris in a macroscale FE model. In this regard, the multiscale method is an alternative for the analysis of the debris due to its high efficiency and accuracy. Multiscale method solves the problems by connecting the macroscale model with the microscale model. The ways of connecting different scale models can be divided into: a) concurrent method, b) hierarchical method and c) semi-concurrent method [Aboudi, Arnold and Bednarcyk (2012)].

In this paper, a semi-concurrent multiscale method is proposed. Through this method, the effect of the debris is analyzed by comparing the difference between microscale models with and without debris. Then, the effective radius is obtained, which is up-scaled from the microscale model to the macroscale model. By changing the radius of the pad in the macroscale model, the effect of the debris can be considered without the need to model it explicitly in the macroscale model after running in stage. Due to the lower number of elements in the microscale model and unnecessity to model debris in the macroscale model, this multiscale approach is more computationally efficient. The macroscale model

passes the wear profile to the microscale model, and then the microscale model passes an effective pad's radius (through analysis of contact pressure) to the macroscale model. The concept used for the semi-concurrent multiscale analysis can be simplified as follows:

$$macroscale\ model \xrightarrow{\text{wear profile}} microscale\ model \xrightarrow{\text{effective pad's radius}} macroscale\ model$$

The paper is organized in the following sequence. After the introduction section, the research background, details of the macroscale and microscale fretting wear models are introduced in Section 2 and Section 3, respectively. Then, the multiscale method that links the macroscale model to microscale model is presented in Section 4. Thereafter, the simulation results are presented and compared with the experimental data in Section 5. Finally, the conclusion of this paper is given in Section 6.

2 Theoretical background

2.1 Contact mechanics

Hertzian contact theory is used to calculate the contact pressure distribution for the two elastic contact parts under normal load, which was originally proposed by Hertz [Hertz (1882)]. Hertzian contact is derived based on the following assumptions: 1) no plastic deformation, 2) the dimensions have no limitation on the stress distribution and 3) there is no friction between the contact surfaces. Two elastic bodies with curved surfaces under normal load were analyzed in Johnson et al. [Johnson and Johnson (1987); Popov (2010)].

A cylinder on cylinder configuration is considered as an example to show the distribution of the contact pressure, which is shown in Fig. 1. This contact configuration is called line contact, in which the half-contact width b is derived as:

$$b = 2\left(\frac{2}{\pi}\right)^{\frac{1}{2}}\left(\frac{F}{L}\right)^{\frac{1}{2}}\left(\frac{R^*}{E^*}\right)^{\frac{1}{2}} \tag{1}$$

where F is normal load, L is contact length, R^* is equivalent radius and E^* is effective Young's modulus. R^* and E^* are given by:

$$\frac{1}{R^*} = \frac{1}{R_1} + \frac{1}{R_2} \tag{2}$$

$$\frac{1}{E^*} = \frac{1-\nu_1^2}{2E_1} + \frac{1-\upsilon_2^2}{2E_2} \tag{3}$$

where R_1 and R_2 are the radii, E_1 and E_2 are Young's moduli and ν_1 and ν_2 are the Poisson's ratios of two cylinders respectively.

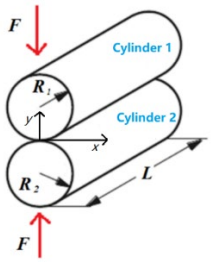

Figure 1: Hertzian contact of cylinder on cylinder configuration

By considering the vertical indentation and the distance between the two surfaces, we can get the pressure distribution along the contact width as:

$$p(x) = p_{max}\sqrt{1-(\frac{x}{b})^2}, \text{ where } p_{max} = \left(\frac{FE^*}{2\pi LR^*}\right)^{\frac{1}{2}} \quad (4)$$

The contact pressure along the contact surface is shown in Fig. 2.

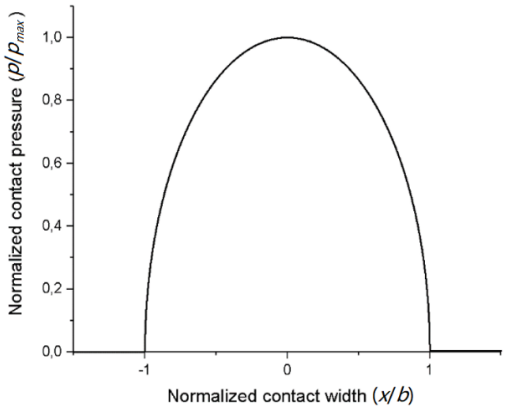

Figure 2: Normalized contact pressure along the normalized contact width

If the radius of the cylinder 2, R_2, approaches infinity, Eq. (2) becomes Eq. (5) and the contact develops into the cylinder on plane contact [Popov (2010)]:

$$\frac{1}{R^*} = \frac{1}{R_1} \quad (5)$$

2.2 Multiscale analysis

Multiscale analysis can be classified into hierarchical method, semi-concurrent method and concurrent method [Budarapu, Gracie, Yang et al. (2014)]. Hierarchical homogenization method is a one-way multiscale method because it can only be used to extract the features from the microscale model and up-scale these features to the macroscopic model [Jafari, Khatibi and Mashhadi (2011); Talebi, Silani, Bordas et al. (2014); Wasselynck, Trichet, Ramdane et al. (2010)]. Kyvia et al. [Pereira, Yue and Wahab (2017)] considered the effect of the roughness of contacting geometries by up-scaling the effect of the roughness from microscale model to the macroscale model. They analyzed the fretting wear in the macroscale model without roughness. Ding et al. [Ding, Leen, Williams et al. (2009)] analyzed the effect of the local asperity on fretting wear process using homogenization of the local plasticity in microscale model and then up-scale the corresponding parameters to the macroscale model.

The semi-concurrent approach is a two-way multiscale method, which means that the results of the microscale model are sent to the macroscale model, and vice versa [Andrade and Tu (2009); Kouznetsova (2002); Silani, Ziaei-Rad, Talebi et al. (2014)]. The procedures of the semi-concurrent method are presented in Fig. 3 [Zhu, Wang and Zhuang (2016)]. Zhu et al. [Zhu, Wang and Zhuang (2016)] proposed a semi-concurrent

method for the crack initiation prediction, in which ε is the strain, L is the homogenized tangential constitutive tensor, and σ is the microscale stress. In the first step, ε in the macroscale model is calculated by the input of L and σ from the microscale model. In the second step, ε from the macroscale model is applied to the microscale model as the boundary condition. Then new L and σ are calculated and used as the new input for the macroscale model. This semi-concurrent process will end when the converged parameters are obatined. Talebi et al. [Talebi, Silani, Bordas et al. (2014)] proposed a software PERMIX to solve the semi-concurrent FE-FE coupling for the nanocomposite.

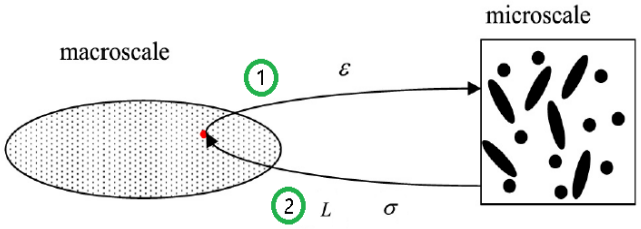

Figure 3: Schematic diagram of the semi-concurrent approach [Zhu, Wang and Zhuang (2016)]

The concurrent method can solve the fully coupled macroscale model and microscale model at one time, which is computationally expensive [Broughton, Abraham, Bernstein et al. (1999); Iacobellis and Behdinan (2013); Muralidharan, Deymier and Simmons (2003); Su, Tan and Tay (2012); Wagner and Liu (2003)]. The boundary conditions and the interface between the multiscale models are very important for the application of this method. Iacobellis et al. [Iacobellis and Behdinan (2013)] classified the concurrent methods into the direct coupling and handshake coupling method, which is commonly used to connect continuum elements to atoms. For the direct coupling, the displacement boundary conditions enforce the FE nodes to move with the atoms. While in the handshaking coupling, the FE nodes and the atoms are not located in the same position to avoid resolving the FE mesh with the atoms on the interface [Broughton, Abraham, Bernstein et al. (1999)]. Talebi et al. [Talebi, Silani and Rabczuk (2015)] modeled 3D crack propagation and dislocation by bridging domain method, which coupled atoms with extended finite elements in handshaking domain. Besides the bridging domain method, Budarapu et al. [Budarapu, Gracie, Yang et al. (2014)] proposed an adaptive multiscale method that can couple the molecular dynamics and continuum element with the coarse scale domain existing everywhere. Concurrent method can also be used to couple FE-FE model. Silani et al. [Silani, Talebi, Ziaei-Rad et al. (2015)] proposed an extended Arlequin method to couple to continuum domains to analyze dynamic fracture, which is mainly based on linear energy weighting in the overlapping domain.

3 Fretting wear models

3.1 Macroscale model

The dimensions and the boundary conditions of the 2D macroscale model in ABAQUS are shown in Fig. 4, based on the data from McColl et al. [McColl, Ding and Leen (2004); Yue and Wahab (2014)]. In ABAQUS, the fretting wear pad and specimen are modelled at macroscale level using three parts: pad, contact specimen part (CSP) and base specimen part (BSP). CSP and BSP are connected by the constraint TIE to make it possible to import the CSP from the macroscale model to the microscale model. The 4-node bilinear plane strain quadrilateral (CPE4) element is assigned for all parts in the model. A finer mesh is applied to the contact zone, i.e., partition of the pad and CSP. The normal load P is applied at the top centre of the pad in the first load step. Then, the oscillatory displacement, D=25 μm, is applied at the same position in the following load steps. After reaching the final number of cycles, i.e., 18000 cycles, the normal load is set to zero to obtain the un-deformed wear profile, which is namely a releasing load step. The loading process is shown in Fig. 5. Moreover, the MPC (Multi-Point Constraint) is exerted on the top of the pad, and the bottom of the BSP is fixed, which means that the displacement along x and y direction and rotation along z axis are all set to zero. The CSP is set as the ALE (Arbitrary Lagrangian-Eulerian) adaptive meshing domain, in which the mesh of the domain moves independently of the material. The properties of the material used for both pad and specimen, i.e., super CMV steel, are listed in Tab. 1, which is taken from McColl et al. [McColl, Ding and Leen (2004)].

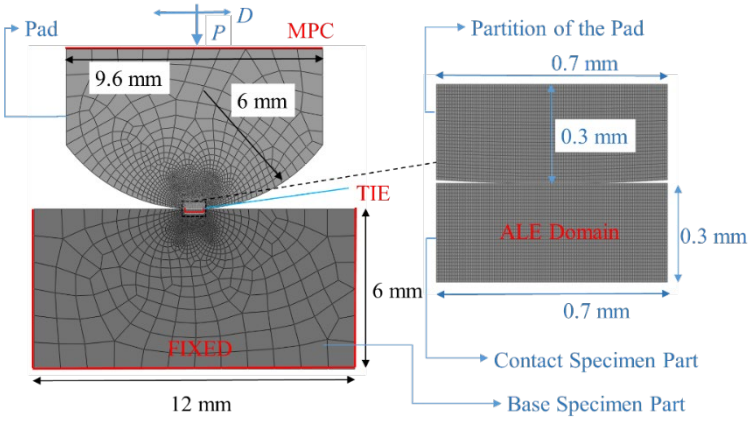

Figure 4: Dimensions and boundary conditions of the macroscale model

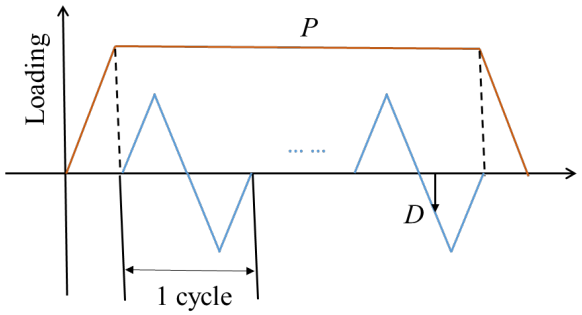

Figure 5: Loading process of the macroscale model

Table 1: Material property

E	Young's modulus (GPa)	200
ν	Poisson's ratio	0.3

Surface to surface contact is created between the cylinder partition and the CSP. Lagrange Multiplier is used as the friction formulation for the tangential behavior of the contact. The calculation of the wear on the surface of CSP is based on the dissipated energy equation. The local wear depth is obtained by:

$$\Delta h_i = K_E \int_0^T q_i(x) ds_i(x) \tag{6}$$

where the subscript i means the i^{th} cycle, T is the period for one cycle, μ is the coefficient of friction (CoF), K_E is the energy wear coefficient, $ds_i(x)$ and $q_i(x)$ are the slip and the shear stress at the x position respectively, and Δh_i is the local wear depth. This calculation is performed by using the subroutine UMESHMOTION after every increment in ABAQUS, which is coded in FORTRAN language. The wear depth is calculated on every node on the surface of the ALE domain after each load increment. Then, the mesh is updated based on the calculated wear depth. To make the simulation process more efficient, jump cycles ΔN=1000 cycles is used to reduce the effective cycles in ABAQUS. The CoF, μ, between the contact surfaces and wear coefficient K_E under the normal load P are listed in Tab. 2, which are derived from McColl et al. [McColl, Ding and Leen (2004); Yue and Wahab (2014)].

Table 2: Normal load, CoF and wear coefficient

P (N)	μ	K_E (MPa^{-1})
185	0.88	3.3×10^{-8}

In fretting process, both generation and ejection of debris occur. To determine the wear kinetics in fretting process, a reference wear kinetics model is used as shown in Fig. 6 [Done, Kesavan, Chaise et al. (2017)].

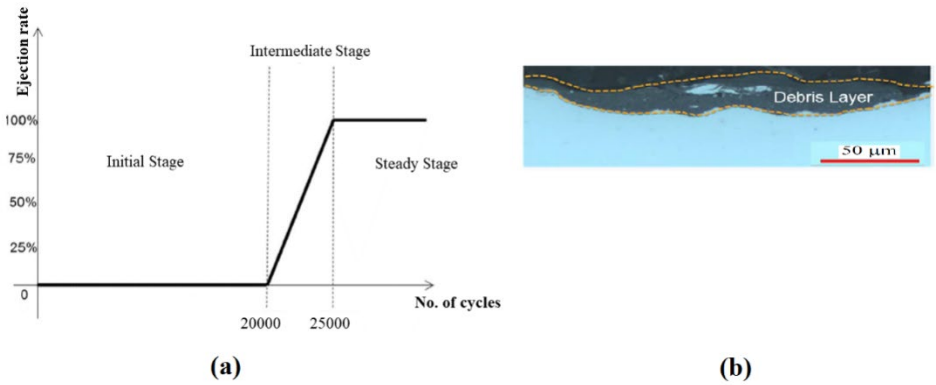

Figure 6: Referenced wear kinetics: (a) ejection rate in the fretting process and (b) cross-sectional image showing debris layer after 100000 cycles [Done, Kesavan, Chaise et al. (2017)]

As shown in Fig. 6(a), in the initial stage, the ejection rate of the debris is almost zero. Through the intermediate stage, the ejection rate tends to be 100%, which means that the ejection of the debris is equal to the generation of the debris. After 100000 cycles, a cross-sectional image of the debris layer is shown in Fig. 6(b). In this paper, the total number of cycles is 18000. Considering the wear kinetics shown in Fig. 6, the effect of the debris is analyzed after the running in stage N_R=3000 cycles in the overall 18000 cycles, which is defined in Yue et al. [Yue and Wahab (2016)]. In the running in stage, the effect of the debris is neglected due to its little influence.

3.2 Microscale model

The microscale model is created after N_R cycles, and is shown in Fig. 7. The cylindrical part (CP) has the same dimension as the partition of the pad shown in Fig. 4. CPE4 element is also used in whole microscale model. The CSP in the microscale model is imported from the macroscale model after N_R with the wear profile. The time point of introducing the CSP from the macroscale model to the microscale model is shown in Fig. 8. The dimensions, load and boundary conditions in microscale model without debris, shown in Fig. 7(b), are the same as those shown in Fig. 7(a). The Normal load P is applied on the top centre of the CP and MPC is applied on the top of the CP. The displacement along the x direction (U1) is set to zero in the normal loading step. The bottom of the CSP is fixed. The boundary conditions are validated by comparing the contact pressure of the microscale model and macroscale model after N_R as shown in Fig. 15 (see Section 4). The geometry of the debris layer is based on the wear profile of the CSP, which is shown in Fig. 9 [Yue and Wahab (2016)]. The normal load in the microscale model is the same as that in the macroscale model.

As is shown in Fig. 9, for the microscale model with the debris layer, two contact interferences are defined for the top and bottom of the debris layer. The CoF between the CP and debris is set as 1, while the CoF between the CSP and debris layer is set as 0.88 [Yue and Wahab (2016)].

The material of the debris layer is $\alpha - Fe_2O_3$, which is different from pad and specimen [Yue and Wahab (2016)]. The material properties of the debris layer are listed in Tab. 3. The thickness of the debris is assumed to be 5 μm, which is based on Section 5.3 (see later).

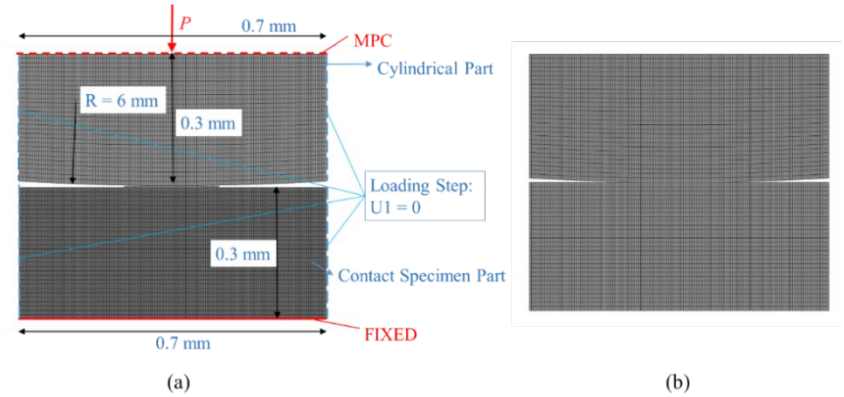

Figure 7: Microscale models details: (a) with debris and (b) without debris

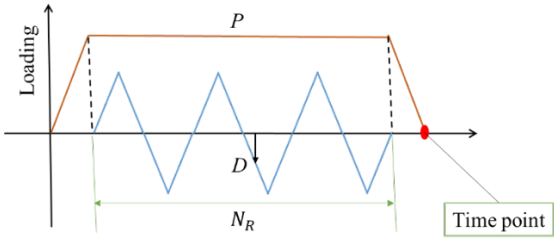

Figure 8: The time point of introducing the CSP from the macroscale model to the microscale model

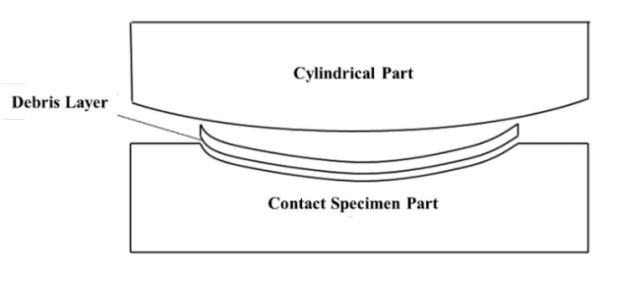

Figure 9: Schematic diagram of debris layer between the CP and CSP

Table 3: Material property of the debris layer

E	Young's modulus (GPa)	360
ν	Poisson's ratio	0.12

4 Semi-concurrent multiscale model

To analyse the effect of the debris, the contact pressures of the microscale model with and without debris are shown in Fig. 10. After the introduction of the debris layer, contact pressure irregularity occurs. To eliminate the irregularity in the contact pressures and make them comparable, kernel smoothing method is applied to the microscale model with the debris. The radial basis function kernel is used for smoothing [Friedman, Hastie and Tibshirani (2001)]. The kernel smoothing method is available in Python. The contact pressure for the model without debris and the kernel-smoothed contact pressure of the model with debris are shown in Fig. 11. From Fig. 11, we can see that the stress irregularity is eliminated by the kernel smoothing. In this way, the maximum contact pressures shown in Fig. 11 are comparable.

Based on Eqs. (1)-(5), we have:

$$R = \frac{FE^*}{\pi L p_{max}^2} \tag{7}$$

where R is equal to the radius of the pad. Because F, $E^*$and L in Eq. (7) are constant in microscale model, the relation between R and p_{max} is written as:

$$R \propto \frac{1}{p_{max}^2} \tag{8}$$

The effective radius of the microscale model with debris is given by:

$$\frac{R_W}{R_{Nef}} \propto \frac{p_{Nmax}^2}{p_{Wmax}^2} \tag{9}$$

where p_{Nmax} and R_{Nef} are the maximum contact pressure and the original radius of the pad in the model without debris, respectively, while p_{Wmax} and R_W are the maximum kernel-smoothed contact pressure and effective radius in microscale model with debris, respectively. p_{Nmax} and p_{Wmax} are obtained from Fig. 11. The values of p_{Nmax}, R_{Nef}, p_{Wmax} and R_W are presented in Tab. 4. The flowchart of the semi-concurrent multiscale model is shown in Fig. 12, in which N_{TC} is the total number of cycles.

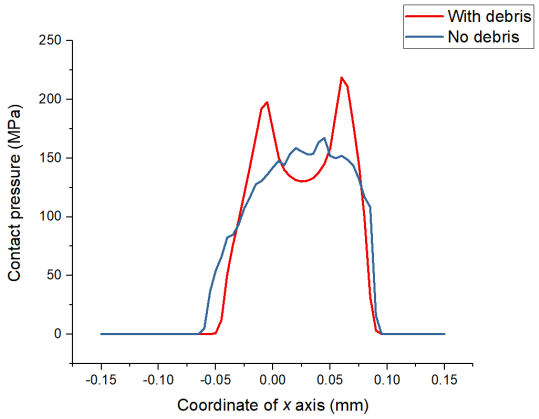

Figure 10: Contact pressures difference between the microscale models with and without debris after N_R cycles

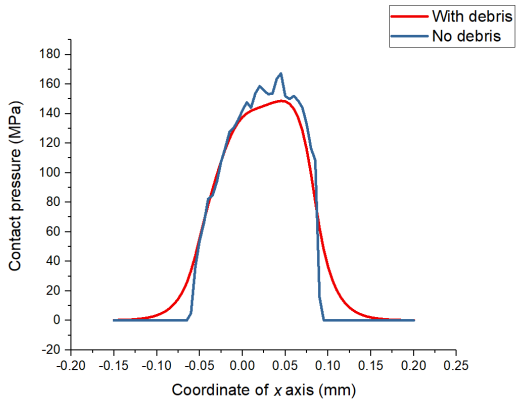

Figure 11: The contact pressure for the model without considering debris and the kernel-smoothed contact pressure of the model with debris

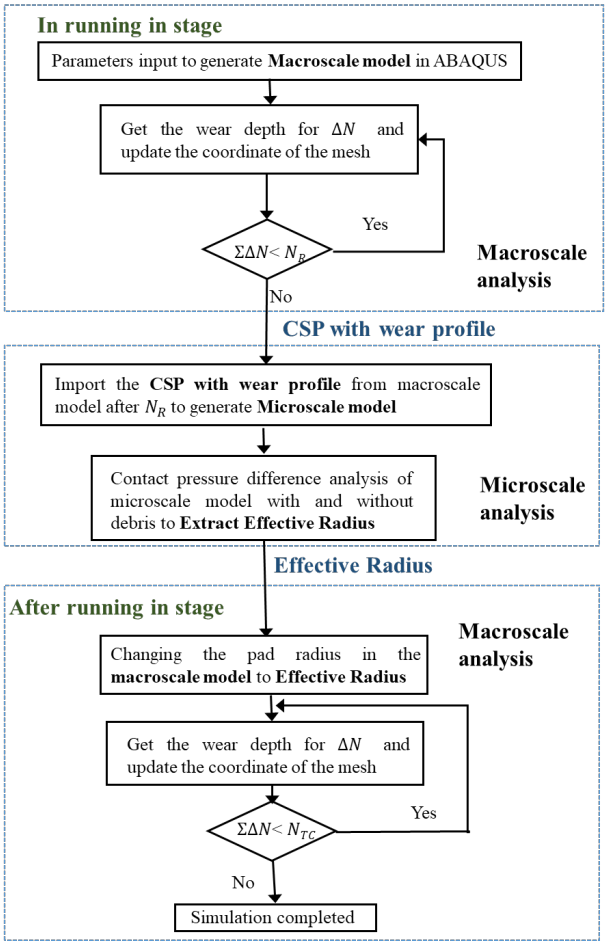

Figure 12: Flowchart of the semi-concurrent multiscale model

Table 4: The values of $\boldsymbol{p_{Nmax}}$, $\boldsymbol{R_{Nef}}$, $\boldsymbol{p_{Wmax}}$ and $\boldsymbol{R_W}$ in microscale model with and without debris

p_{Nmax}	Max contact pressure (MPa)	167.2
R_{Nef}	Original radius (mm)	6.0
p_{Wmax}	Kernel-smoothed Max contact pressure (MPa)	148.6
R_W	Effective radius (mm)	7.6

5 Results and discussion

5.1 Verification of the models

FE models should be validated before using them to study the effect of debris. The contact pressure distribution along the specimen contact surface is calculated using the analytical method based on Eqs. (1) to (4). The analytical solution is compared with the output from FE post processing nodal data. The analytical maximum pressure and half-contact width is 328.5 MPa and 0.035 mm, while maximum pressure and the half-contact width of FEM is 328.8 MPa and 0.036 mm, respectively. The comparison between the FE and analytical results are shown in Fig. 13, from which we can see that FE results are in a good agreement with the analytical results. Therefore, the macroscale FE model is feasible for the fretting wear analysis.

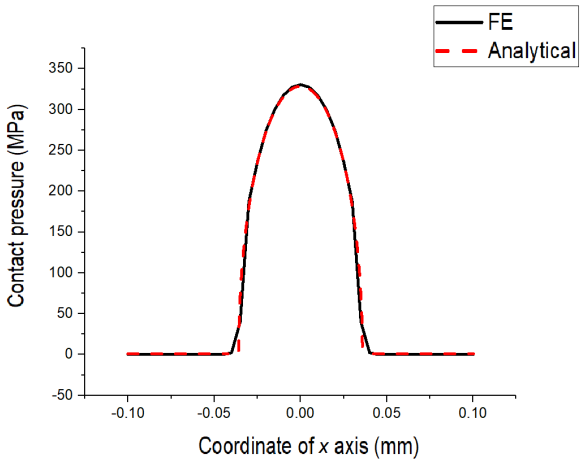

Figure 13: Contact pressure of FEM and analytical method in macroscale model

Moreover, the wear profile of the macroscale fretting wear model after 18000 cycles are compared with results of simulations in Yue et al. [Yue and Wahab (2016)], as shown in Fig. 14. By comparing the wear profiles, it is concluded that the wear simulation result of the macroscale model has a good agreement with that of the reference model. Therefore, the boundary conditions, dimensions and the load of the macroscale model are suitable for fretting wear analysis.

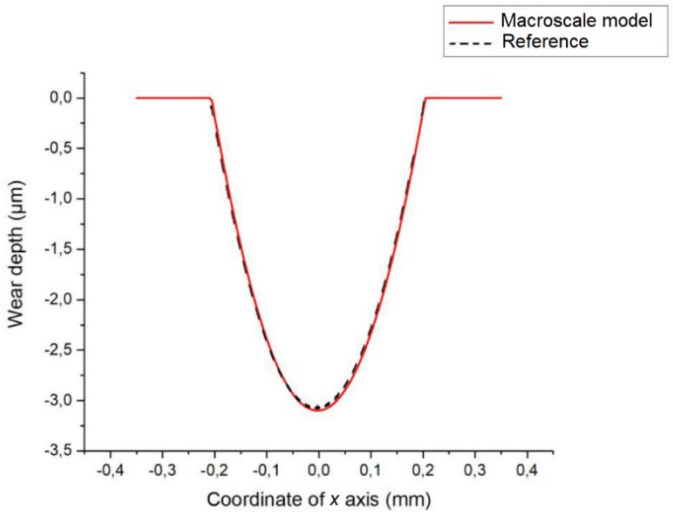

Figure14: Wear profiles of macroscale model and the referenced FE model after 18000 cycles [Yue and Wahab (2016)]

In the microscale model, the contact pressure is used to analyse the effect of debris after N_R. Therefore, the contact pressure in macroscale model after N_R is compared with that in the microscale model without debris under normal load P to verify the dimensions and boundary conditions shown in Fig. 7. The contact pressure in the macroscale model after N_R and in the microscale model without debris are shown in Fig. 15, from which it is concluded that the contact pressures are in a good agreement (the difference is less than 2%). Therefore, the dimension and boundary conditions of the microscale scale model are suitable for contact pressure analysis.

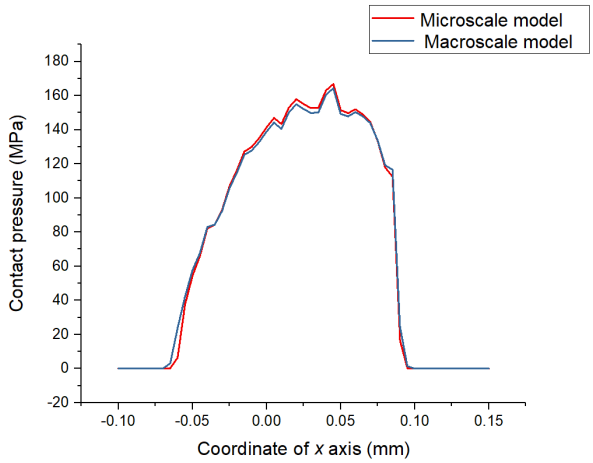

Figure 15: Comparison of contact pressure between the macroscale model after N_R cycles and microscale model without debris

5.2 Experimental validation of the wear profile

The wear profile of the multiscale model is compared with that of the macroscale model after 18000 cycles, as shown in Fig. 16. Based on Fig. 16, it is clearly seen that the wear depth of the multiscale model with debris is lower than that of the macroscale model without debris, while the wear width of the multiscale model is higher.

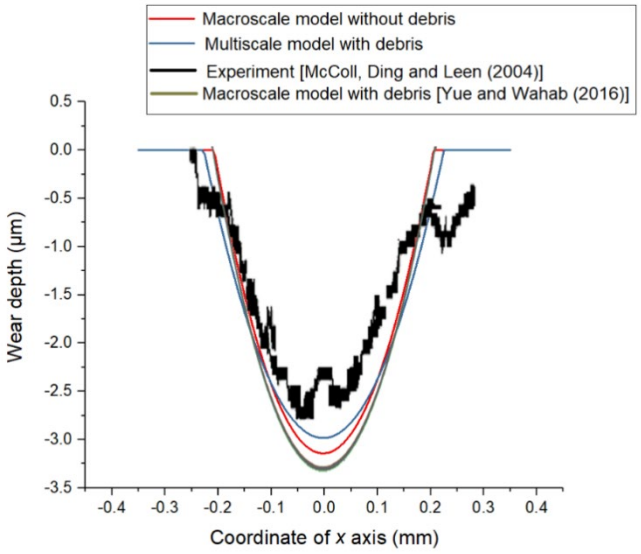

Figure 16: Comparison of wear profile between the multiscale model with debris and macroscale model without debris after 18000 cycles

Table 5: Wear profile characteristics of the multiscale model and macroscale model, and the experimental data [McColl, Ding and Leen (2004)] after 18000 cycles

Wear characteristics	Multiscale model with debris	Macroscale model without debris	Experiments data
Wear depth (μm)	2.98	3.14	2.90
Wear width (mm)	0.46	0.41	0.54
Wear volume ($mm^3/10^3$)	0.896	0.864	0.900

McColl et al. [McColl, Ding and Leen (2004)] did the fretting wear experiments under different loading conditions and measured the profile characteristics of the wear scar. The wear profile characteristics of the multiscale model with debris and macroscale model without debris, and the experimental data after 18000 cycles are presented in Tab. 5. To make the differences seem more intuitive, the difference between these two models and experimental wear characteristics are shown in Fig. 17, in which the experimental data is set as 1 [McColl, Ding and Leen (2004)]. From Fig. 17, it is concluded that though small differences exist, the wear profile characteristics of the multiscale model have a better agreement with the experimental results than those of the macroscale model.

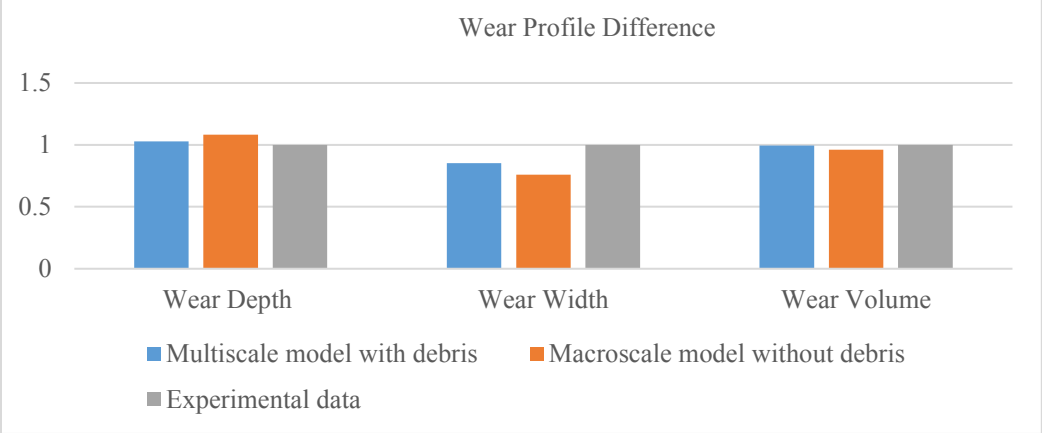

Figure 17: The difference between multiscale model with debris, macroscale model without debris and experimental results [McColl, Ding and Leen (2004)]

5.3 Effect of the debris layer thicknesses

The effect of the debris thicknesses is shown in Fig. 18, from which, we can see that with the increment of the debris layer thickness, the maximum contact pressure decreases.

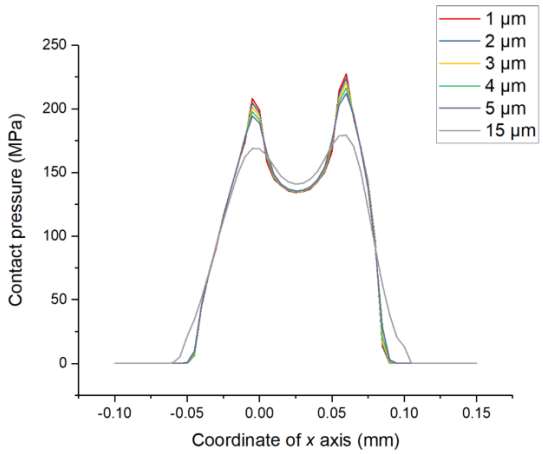

Figure 18: The contact pressure of microscale model with different thicknesses of debris

To analyze the effect of the debris, the effective radius is obtained by kernel smoothing method as before. Therefore, the kernel-smoothed contact pressures of the microscale model with different thicknesses are compared, as shown in Fig. 19. The maximum kernel-smoothed contact pressures show little difference (less than 3%). Because the debris thickness has a little effect on the kernel-smoothed contact pressure, herein, 5 μm is selected as the thickness of the debris layer in the microscale model.

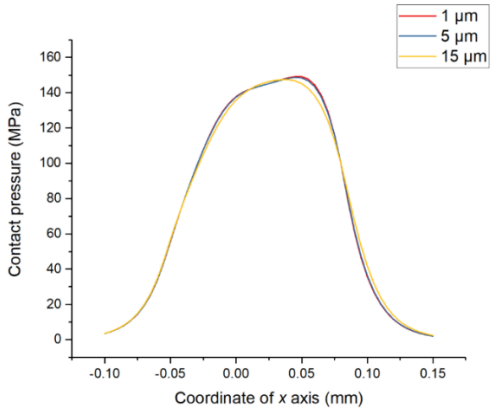

Figure 19: Kernel-smoothed contact pressures of the microscale model with different thicknesses

5.4 The efficiency of the multiscale analysis

To get an effective radius, the normal load is applied to the microscale model with debris. To analyze the efficiency of the multiscale analysis, CPU time of normal loading step after N_R cycles in the microscale model with the debris is compared with that in the macroscale model with debris layer. The results are shown in Tab. 6. Based on Tab. 6, it is clearly seen that using the multiscale method, the CPU time of normal loading step in the microscale model with debris is quite lower than that in the macroscale model with debris due to the smaller number of elements used in microscale model.

Table 6: Comparison of CPU time of normal loading step after $\boldsymbol{N_R}$ between the microscale model with debris and the macroscale model with debris

Model	CPU time (s)
Microscale model with debris	72.6
Macroscale model with debris	165.9

By the multiscale approach, the effect of the debris is considered without the need to model the debris layer in macroscale model after N_R cycles. Therefore, the CPU time of one cycle in the macroscale model with debris is compared with that in the macroscale model without debris. The results are shown in Tab. 7. From Tab. 7, we can see that one cycle CPU time of the macroscale model with debris is more than 2 times larger than that in the macroscale model without debris.

Table 7: Comparison of CPU time of one cycle after $\boldsymbol{N_R}$ between the macroscale model with debris and macroscale model without debris

Model	CPU time (s)
Macroscale model with debris	476.8
Macroscale model without debris	195.9

6 Conclusion

In this paper, the effect of the debris is analysed by the semi-concurrent multiscale method. In this method, the debris kinetics is considered. By comparing the result of the multiscale model with the macroscale model, it is concluded that the wear profile of the multiscale model shows a better agreement with experiments than that of the macroscale model without considering debris. Due to the smaller number of elements in the microscale model and unnecessity to model the debris in the macroscale model after N_R cycles, the CPU time of the multiscale method is much lower than that of the macroscale model. This means that the multiscale model shows a high computational efficiency.

References

Aboudi, J.; Arnold, S. M.; Bednarcyk, B. A. (2012): Micromechanics of composite materials: a generalized multiscale analysis approach. *Butterworth-Heinemann*.

Achard, J. (1953): Contact and rubbing of flat surface. *Journal of Applied Physics*, vol. 24, no. 8, pp. 981-988.

Andrade, J. E.; Tu, X. (2009): Multiscale framework for behavior prediction in granular media. *Mechanics of Materials*, vol. 41, no. 6, pp. 652-669.

Arnaud, P.; Fouvry, S.; Garcin, S. J. W. (2017): A numerical simulation of fretting wear profile taking account of the evolution of third body layer. *Wear*, vol. 376, pp. 1475-1488.

Berthier, Y.; Vincent, L.; Godet, M. (1989): Fretting fatigue and fretting wear. *Tribology international*, vol. 22, no. 4, pp. 235-242.

Bhatti, N. A.; Pereira, K.; Wahab, M. A. (2018): A comparison between critical-plane and stress-invariant approaches for the prediction of fretting fatigue crack nucleation. *Fracture, Fatigue and Wear*, pp. 530-538.

Bhatti, N. A.; Pereira, K.; Wahab, M. A. (2019): Effect of stress gradient and quadrant averaging on fretting fatigue crack initiation angle and life. *Tribology International*, vol. 131, pp. 212-221.

Bhatti, N. A.; Wahab, M. A. (2018a): Fretting fatigue crack nucleation: a review. *Tribology International*, vol. 121, pp. 121-138.

Bhatti, N. A.; Wahab, M. A. (2018b): Fretting fatigue damage nucleation under out of phase loading using a continuum damage model for non-proportional loading. *Tribology International*, vol. 121, pp. 204-213.

Broughton, J. Q.; Abraham, F. F.; Bernstein, N.; Kaxiras, E. (1999): Concurrent coupling of length scales: methodology and application. *Physical Review B*, vol. 60, no. 4, pp. 2391.

Budarapu, P. R.; Gracie, R.; Yang, S. W.; Zhuang, X.; Rabczuk, T. (2014): Efficient coarse graining in multiscale modeling of fracture. *Theoretical and Applied Fracture Mechanics*, vol. 69, pp. 126-143.

Budarapu, P. R.; Gracie, R.; Bordas, S. P.; Rabczuk, T. (2014): An adaptive multiscale method for quasi-static crack growth. *Computational Mechanics*, vol. 53 no. 6, pp. 1129-1148.

Ding, J.; Leen, S.; Williams, E.; Shipway, P. (2009): An asperity-contact based oxidation model for fretting wear with the presence of debris. *Advanced Tribology*, pp. 346-347.

Ding, J.; McColl, I., Leen, S.; Shipway, P. (2007): A finite element based approach to simulating the effects of debris on fretting wear. *Wear*, vol. 263, no. 1-6, pp. 481-491.

Done, V.; Kesavan, D.; Chaise, T.; Nelias, D. (2017): Semi analytical fretting wear simulation including wear debris. *Tribology International*, vol. 109, pp. 1-9.

Fouvry, S.; Duo, P.; Perruchaut, P. (2004): A quantitative approach of Ti-6Al-4V fretting damage: friction, wear and crack nucleation. *Wear*, vol. 257, no. 9-10, pp. 916-929.

Friedman, J.; Hastie, T.; Tibshirani, R. (2001): The elements of statistical learning. *New York Springer Series in Statistics*, vol. 1, no. 10.

Hertz, H. (1882): Über die Berührung fester elastischer Körper und über die Harte. *Gesammelte Werke*, Bd, 1.

Hills, D. A. (1994): Mechanics of fretting fatigue. *Wear*, vol. 175, no. 1-2, pp. 107-113.

Iacobellis, V.; Behdinan, K. (2013): Comparison of concurrent multiscale methods in the application of fracture in nickel. *Journal of Applied Mechanics*, vol. 80, no. 5, 051003.

Jafari, A.; Khatibi, A. A.; Mashhadi, M. M. (2011): Comprehensive investigation on hierarchical multiscale homogenization using representative volume element for piezoelectric nanocomposites. *Composites Part B: Engineering*, vol. 42, no. 3, pp. 553-561.

Johnson, K. L.; Johnson, K. L. (1987): *Contact Mechanics*. Cambridge University Press.

Klaffke, D. (1989): Fretting wear of ceramics. *Tribology International*, vol. 22, no. 2, pp. 89-101.

Kouznetsova, V. (2004): *Computational Homogenization for The Multi-Scale Analysis of Multi-Phase Materials (PhD thesis)*. Technische Universiteit Eindhoven, The Netherland.

McColl, I.; Ding, J.; Leen, S. (2004): Finite element simulation and experimental validation of fretting wear. *Wear*, vol. 256, no. 11-12, pp. 1114-1127.

Muralidharan, K.; Deymier, P.; Simmons, J. H. (2003): A concurrent multiscale finite difference time domain/molecular dynamics method for bridging an elastic continuum to an atomic system. *Modelling and Simulation in Materials Science and Engineering*, vol. 11, no. 4, pp. 487.

Ovcharenko, A.; Etsion, I. (2009): Junction growth and energy dissipation at the very early stage of elastic-plastic spherical contact fretting. *Journal of Tribology*, vol. 131, no. 3, 031602.

Paulin, C.; Fouvry, S.; Deyber, S. (2005): Wear kinetics of Ti-6Al-4V under constant and variable fretting sliding conditions. *Wear*, vol. 259, no. 1-6, pp. 292-299.

Paulin, C.; Fouvry, S.; Meunier, C. (2008): Finite element modelling of fretting wear surface evolution: Application to a Ti-6A1-4V contact. *Wear*, vol. 264, no. 1-2, pp. 26-36.

Pereira, K.; Wahab, M. (2018): Effect of short crack behavior on the propagation life prediction for a fretting cylindrical pad configuration. *Fracture, Fatigue and Wear*, pp.

539-546.

Pereira, K.; Wahab, M. A. (2017): Fretting fatigue crack propagation lifetime prediction in cylindrical contact using an extended MTS criterion for non-proportional loading. *Tribology International*, vol. 115, pp. 525-534.

Pereira, K.; Yue, T.; Wahab, M. A. (2017): Multiscale analysis of the effect of roughness on fretting wear. *Tribology International*, vol. 110, pp. 222-231.

Popov, V. L. (2010): *Contact Mechanics and Friction*, pp. 231-253. Springer Berlin Heidelberg,

Silani, M.; Ziaei-Rad, S.; Talebi, H.; Rabczuk, T. (2014): A semi-concurrent multiscale approach for modeling damage in nanocomposites. *Theoretical and Applied Fracture Mechanics*, vol. 74, pp. 30-38.

Silani, M.; Talebi, H.; Ziaei-Rad, S.; Hamouda, A. M.; Zi, G. et al. (2015): A three dimensional extended Arlequin method for dynamic fracture. *Computational Materials Science*, vol. 96, pp. 425-431.

Su, Z.; Tan, V.; Tay, T. (2012): Concurrent multiscale modeling of amorphous materials in 3D. *International Journal for Numerical Methods in Engineering*, vol. 92, no. 13, pp. 1081-1099.

Talebi, H.; Silani, M.; Bordas, S. P.; Kerfriden, P.; Rabczuk, T. (2014): A computational library for multiscale modeling of material failure. *Computational Mechanics*, vol. 53, no. 5, pp. 1047-1071.

Talebi, H.; Silani, M.; Rabczuk, T. (2015): Concurrent multiscale modeling of three dimensional crack and dislocation propagation. *Advances in Engineering Software*, vol. 80, pp. 82-92.

Van Beek, A. (2015): *Advanced Engineering Design*, pp. 191-192. TU Delft, Delft, The Netherlands.

Wagner, G. J.; Liu, W. K. (2003): Coupling of atomistic and continuum simulations using a bridging scale decomposition. *Journal of Computational Physics*, vol. 190, no. 1, pp. 249-274.

Wasselynck, G.; Trichet, D.; Ramdane, B.; Fouldagar, J. (2010): Interaction between electromagnetic field and CFRP materials: a new multiscale homogenization approach. *Transactions on Magnetics*, vol. 46, no. 8, pp. 3277-3280.

Yue, T.; Abdel Wahab, M. (2016): A numerical study on the effect of debris layer on fretting wear. *Materials*, vol. 9, no. 7, pp. 597.

Yue, T.; Wahab, M. A. (2017): Finite element analysis of fretting wear under variable coefficient of friction and different contact regimes. *Tribology International*, vol. 107, pp. 274-282.

Yue, T.; Wahab, M. A. (2014): Finite element analysis of stress singularity in partial slip and gross sliding regimes in fretting wear. *Wear*, vol. 321, pp. 53-63.

Zhu, H.; Wang, Q.; Zhuang, X. (2016): A nonlinear semi-concurrent multiscale method for fractures. *International Journal of Impact Engineering*, vol. 87, pp. 65-82.